Arch. Met. Geoph. Biocl., Ser. B, 32, 111–129 (1983)

ARCHIVES
FOR METEOROLOGY,
GEOPHYSICS, AND
BIOCLIMATOLOGY

551.521

Institut für Meteorologie, Johannes Gutenberg-Universität Mainz,
Mainz, Federal Republic of Germany

An Approximate Calculation Method for Parallel and Diffuse Solar Irradiances on Inclined Surfaces in the Presence of Obstructing Mountains or Buildings

Chr. Brühl and **W. Zdunkowski**

With 5 Figures

Received December 20, 1982

Summary

This paper presents an approximate theoretical method to calculate solar irradiances received by inclined surfaces in mountain valleys or city streets. Results can be used in mesoscale and urban dynamic modelling.
The calculation scheme requires parallel and diffuse radiative flux densities at the lower boundary of the atmosphere on horizontal unobstructed surfaces. Because of numerical efficiency these quantities may be calculated from any reliable two-stream method or extracted from available measurements. Complex yet computationally very efficient transformations are presented to handle various model geometries. Multiple reflections between obstacles and the receiving surface are accounted for whenever required. Capability and versatility of the model are demonstrated by considering some special situations in the MESOKLIP-region (Oberrhein), in the Alpine Dischma valley and in city street cavities on the basis of a locally developed two-stream method. It is shown that ignoring obstructions in the treatment of the diffuse sky radiation may lead to serious errors.

Zusammenfassung

Eine approximative Methode zur Berechnung von parallelen und diffusen solaren Bestrahlungsstärken auf geneigten Flächen in Gegenwart von abschattenden Bergen oder Gebäuden

Diese Arbeit stellt eine approximative theoretische Methode zur Berechnung von solaren Bestrahlungsstärken auf geneigten Flächen in Gebirgstälern oder Stadtstraßen vor. Die Ergebnisse können für dynamische Mesoscale- und Stadtmodelle benutzt werden.
Das Rechenverfahren erfordert die Kenntnis paralleler und diffuser Strahlungsflußdichten am Unterrand der Atmosphäre auf horizontalen, nicht abgeschatteten Flächen. Diese Größen können der numerischen Effizienz wegen einem beliebigen, zuverlässigen Zwei-

0066-6424/83/0032/0111/$ 03.80

Strom-Verfahren oder vorliegenden Messungen entnommen werden. Die Flußdichten werden nun mittels umfangreichen aber numerisch sehr leistungsfähigen und effektiven Transformationen auf verschiedene Modellgeometrien umgerechnet. Mehrfachreflexionen zwischen den abschattenden Objekten und der Empfangsfläche werden berücksichtigt, falls erforderlich.
Tauglichkeit und Vielseitigkeit des Modells werden anhand einiger spezieller Situationen im MESOKLIP-Gebiet (Oberrhein), im alpinen Dischmatal und in Stadtstraßen vorgeführt, wobei ein lokal entwickeltes solares Zwei-Strom-Verfahren zur Verwendung kommt. Es wird gezeigt, daß eine Vernachlässigung der Abschattung von diffuser Himmelsstrahlung zu bedeutenden Fehlern führen kann.

1. Introduction

Recently, Zdunkowski (Z) et al. [17] and Welch and Zdunkowski (WZ) [14] presented approximate calculation methods to obtain direct and diffuse solar flux densities on inclined surfaces for arbitrary atmospheres. While the previous studies considered isolated sloping surfaces, the present work considers additionally the effect of obstructions caused by neighboring mountains or buildings.
For a horizontal receiving element and isotropic diffuse radiation Junghans [7] gives equations which determine the obstructing effect of a neighboring slope. He also gives some analytical formulas which handle the obstruction of parallel radiation. His method, however, is not general enough for mesoscale modelling. In contrast to the analytical scheme Escher-Vetter [4] introduced numerical procedures to treat the shadowing effects of mountains to the incoming parallel solar radiation. The present model uses some of Escher-Vetter's ideas in treating parallel radiation but employs a new method to account for obstruction of diffuse radiation in arbitrary atmospheres even in the presence of multilayered partial cloudiness. This new scheme is capable, for example, to calculate solar illumination for vineyards in the Rhine- and the Mosella valley. To make the analysis possible, it is assumed that the valley is horizontally infinitely far extended, an assumption which is approximately valid for many actual situations. As an immediate application the model is used to calculate the illumination for a selected part of the MESOKLIP region, for the idealized Dischma valley and within a city street.
Various other studies with similar intent appear in the literature. For the special case of a street canyon Aida [1] and Aida and Gotoh [2] present very interesting measurements and calculations for the average street albedo using a block model. However, their Monte Carlo treatment of multiple reflections requires a very high numerical effort. These authors do not present flux densities on receiving elements inside the street cavity. Their approximation of the radiation is based on empirical evidence.

The illumination of buildings and city streets is also investigated by Terjung and O'Rourke [12] and by O'Rourke and Terjung [11]. In their model, obstruction to diffuse sky radiation is described by sky view factors obtained numerically in contrast to the integration method of the present paper. Their treatment is used in conjunction with a heat balance model to obtain temperature distributions in urban areas. In contrast, the present scheme is intended to be used as part of existing dynamic mesoscale and urban models. For this reason the present calculation scheme is devised to be numerically very efficient.

2. Theory

In order to guarantee a uniform notation, the major symbols will be listed first:

F	diffuse irradiance (flux density) on an inclined obstructed surface
L	azimuthally averaged radiance
τ	optical thickness of clouds and aerosol at wavelength 0.55 μm
θ, ϕ	zenith and azimuthal angle of incident radiation
i, b	inclination and azimuthal angle of the receiving slope
α, β	obstruction angles (see Fig. 1)
$F\downarrow, F\uparrow$	downward and upward flux density on a horizontal surface
S_h, S	parallel irradiance (flux density) on a horizontal, an inclined surface
θ_0, ϕ_0	solar zenith and azimuthal angle

Azimuthal angles are measured from south.

2.1 The Obstruction Geometry

Using the notation of Z [17] and WZ [14] the diffuse flux density on an inclined plane is given by

$$F(\tau, i, \alpha, \beta) = \int_0^{2\pi} \int_0^{\theta_L(\phi, i, \alpha, \beta)} L(\tau, \theta) \{\cos\theta \cos i + \sin\theta \sin i \cos(\phi - b)\} \sin\theta \, d\theta \, d\phi$$

$$= \sum_{J=1}^{10} F_J(\tau, i, \alpha, \beta) . \qquad (1)$$

The subdivision into ten partial flux densities F_J at point P in Fig. 1 is necessary to carry out the integration of eq. (1) analytically. Two inclined planes touching the highest points of the mountains visible from P define the shadowing or obstruction angles α and β. The model valley represented by the cross-section of this figure is infinitely far extended perpendicular

to the plane of the paper. The energy incident at point P consists of sky radiation ($F_1 = F_2$; $F_5 = F_6$) and the reflected radiation ($F_3 = F_4$; $F_7 = F_8$: $F_9 = F_{10}$) from the valley floor and from the side walls. The occurrence of partial flux densities in pairs is due to the subdivision of space into symmetric regions as shown in Appendix 1 which lists the integration limits for the F_J.

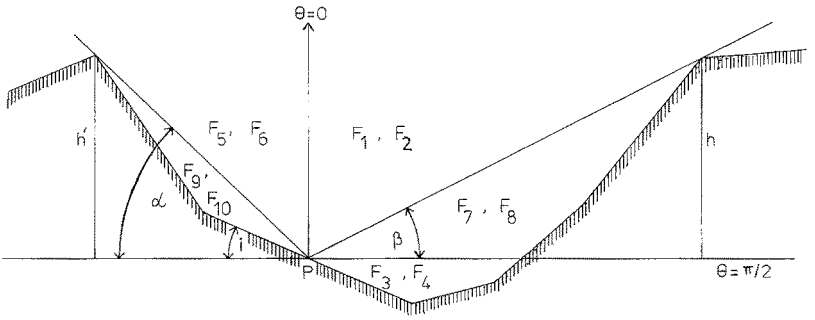

Fig. 1. Geometry of the valley cross-section for calculation of the diffuse partial flux densities F_J. h', h are the heights of the obstructions, defining the shadowing angles α, β; i is the inclination angle of the receiving slope at point P

For practical applications to real valleys the obstructing angles α and β are obtained by a numerical procedure which scans the surrounding mountains, see Appendix 1.

2.2 The Diffuse and Parallel Flux Densities

To obtain the sky radiation the radiance L averaged over the azimuth is approximated as in WZ [14] by a truncated mixed trigonometric series

$$L(\tau, \theta) = \frac{F\downarrow(\tau)}{M} (C_0 + C_1 \sin\theta + C_2 \cos\theta + C_3 \sin^2\theta + C_4 \cos^2\theta) \qquad (2)$$

with the normalization constant $M = \pi(C_0 + \frac{2}{3}[C_1 + C_2] + \frac{1}{2}[C_3 + C_4])$.

In this paper the downward diffuse flux density $F\downarrow(\tau)$ on a horizontal receiving element is calculated with the rather accurate two-stream method (PIFM) described in detail in [15, 16]. Since in this method the strong forward primary scattering is added to the parallel solar radiation, the error due to the assumption of azimuthally independent radiance is strongly reduced. The transformation procedure, however, is not coupled to this particular radiative transfer scheme so that any other reliable two-stream method or even measurements may be used for $F\downarrow(\tau)$.

The coefficients C_K give the best empirical fit to radiances obtained from quasi-exact Monte-Carlo calculations for various optical cloud thicknesses for the functional form adopted in eq. (2). Even though the downward flux density in this equation was originally calculated from PIFM, [14], the resulting integrals in the transformation eq. (1) are not affected by the choice of a particular radiation scheme. It is left up to the potential user of this method either to adopt the C_K given below or to obtain the C_K in some other way. An improved set of C_K (as compared to WZ[1] [14]) as used in this investigation is listed next

$$C_0 = (C + 0.5/C)/1.5 + 0.8/C; \quad C_1 = 0; \quad C_2 = -0.8/C; \qquad (3)$$
$$C_3 = 1/C; \quad C_4 = C\,\mathrm{e}^{-\tau^4/40\,000} \quad \text{with} \quad C = \tau^2/20\,.$$

The next step is to substitute eq. (2) into (1) to obtain the sky radiation for the obstructed inclined plane. A rather complex analytic integration using the limits of integrals listed in Appendix 1 yields the following expressions

$$F_{\mathrm{sky}}\ (\tau, i, \alpha, \beta) = F_1 + F_2 + F_5 + F_6 = \frac{F\downarrow(\tau)}{M} \sum_{K=0}^{4} C_K f_K \qquad (4)$$

with $f_0 = \frac{\pi}{2}(\cos i\,[\cos\alpha + \cos\beta] + \sin i\,[\sin\alpha - \sin\beta])$

$$f_1 = \frac{2}{3}(\cos i\,[\cos^3\alpha\, I(\sin\alpha) + \cos^3\beta\, I(\sin\beta)]$$
$$+ \sin i\,[\frac{1}{\sin\beta}\{\cos^4\beta\, I(\sin\beta) + \cos^2\beta\, K(\sin\beta) - 2E(\sin\beta)\}$$
$$- \frac{1}{\sin\alpha}\{\cos^4\alpha\, I(\sin\alpha) + \cos^2\alpha\, K(\sin\alpha) - 2E(\sin\alpha)\}])$$

$$f_2 = \frac{2}{3}(\cos i\,[\pi - \alpha - \beta + \sin\beta\cos\beta + \sin\alpha\cos\alpha] + \sin i\,[\cos^2\beta - \cos^2\alpha])$$

$$f_3 = f_0 - f_4$$

$$f_4 = \frac{\pi}{8}(\cos i\,[2\{\cos\alpha + \cos\beta\} + \cos\alpha\sin^2\alpha + \cos\beta\sin^2\beta] + \sin i\,[\sin^3\alpha - \sin^3\beta])$$

The function $K(\sin x)$, $E(\sin x)$ and $I(\sin x)$ represent the complete elliptic integrals of the first, second and third kind, respectively. $I(\sin x)$ has the special form

$$I(\sin x) = \int_0^{\pi/2} \frac{\mathrm{d}\,\xi}{(1 - \sin^2 x\,\sin^2\xi)^{3/2}}$$

usually not listed in integration tables.

---

[1] In the paper by WZ [14] a misprint occurred; C_4 should read: $C_4 = C_0\,\exp(-\tau^4/40\,000)$.

For some purposes it might be useful to select $C_1 \neq 0$ so that f_1 was listed for generality.
The radiances needed for the computation of the flux density components originating from the reflecting walls are first assumed to be isotropic in the complete solid angles defined by the integration limits of F_J, i.e.

$$L(\tau) = F\uparrow(\tau)/\pi \,, \tag{5}$$

where $F\uparrow(\tau)$ is obtained from the two-stream method or from measurement for a specified value of the ground albedo. Eq. (5) omits the obstructing effects on the reflected radiation. This deficiency will be remedied lateron.
Again, substituting (5) into eq. (1) gives the flux density F_α from the solid angle defined by the receiving slope and the α-shadowing plane

$$F_\alpha(\tau) = F_9 + F_{10} = \frac{F\uparrow(\tau)}{\pi} \frac{\pi}{2} (1 - \cos i \cos\alpha - \sin i \sin\alpha) \,. \tag{6a}$$

Similarly, the flux density F_β contained in the solid angle between the β-shadowing plane and the receiving slope is calculated from

$$F_\beta(\tau) = F_3 + F_4 + F_7 + F_8 = \frac{F\uparrow(\tau)}{\pi} \frac{\pi}{2} (1 - \cos i \cos\beta + \sin i \sin\beta) \,. \tag{6b}$$

The previous approximation implies the usually small attanuation effect of the atmosphere between the reflecting surfaces and the receiving element is not accounted for due to computational impracticability.
With the definitions of eqs. (3) to (6) the final result for the diffuse flux density on an inclined, obstructed plane is given by

$$F(\tau, i, \alpha, \beta) = \frac{F\downarrow(\tau)}{M} \sum_{K=0}^{4} C_K f_K + F\uparrow(\tau)(1 - f_0/\pi) \,. \tag{7}$$

If the sun is visible from the receiving element, the parallel flux density is calculated from

$$S(\tau, i, b) = S_h(\tau)(\cos i + \sin i \cos(\phi_0 - b) \tan\theta_0) \,, \tag{8}$$

where S_h is taken from the two-stream method or from suitable observational data.

2.3 Multiple Reflection in the Valley

In deep valleys with steep walls or with snow covered ground the isotropic assumption of the previous section is not sufficient. To prevent the multiple reflection calculations from becoming too complicated, it is assumed that the actual valley walls may be represented well by an average cross-section

with straight side-walls. The reflecting walls and the floor of the valley are subdivided into infinitely far extending strips between the gridpoints in the cross-section of Fig. 2. Now the reflected radiance is assumed to be isotropic in each solid angle belonging to each strip l, in the figure referred to point Y_j

$$L_l = \frac{A_l}{\pi}\left(\frac{F_l + F_{l+1}}{2}\right) \quad . \tag{9}$$

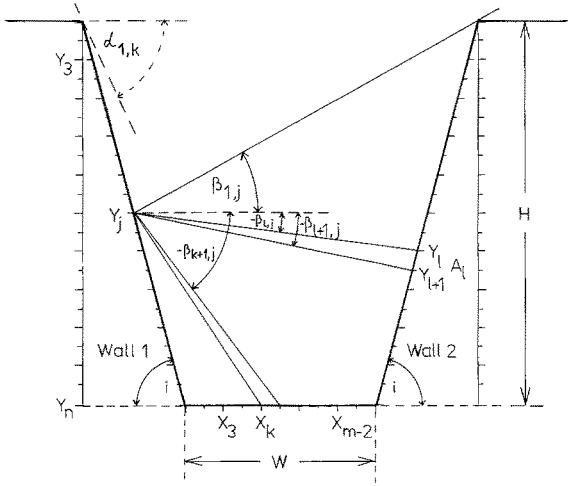

Fig. 2. The grid of an idealized valley cross-section with dimensions W and H. The surface element at height Y_j receives reflected radiation from the strip between Y_l, Y_{l+1} with albedo A_l (see eq. 10). Appendix 2 defines shadowing and limiting angles α and β

F_l and F_{l+1} are the incident irradiances on the gridpoints limiting the strip, A_l is the albedo of the strip.

The integration over each solid angle is simply carried out by substituting eq. (9), instead of (5), into eq. (6b) with the two inclinations $\beta_{l,j}$ and $\beta_{l+1,j}$ of the limiting planes and taking the difference of the results.

Each time reflection takes place the reflected flux density $F_{r,j,1}$ at grid point Y_j at valley wall 1 (Fig. 2) is given by

$$F_{r,j,1} = \pi \sum_{l=1}^{n-1} L_{l,2} \frac{\cos i\,(\cos\beta_{l+1,j} - \cos\beta_{l,j}) - \sin i\,(\sin\beta_{l+1,j} - \sin\beta_{l,j})}{2} + \\ + \pi \sum_{k=1}^{m-1} L_k \frac{\cos i\,(\cos\beta_{k,j} - \cos\beta_{k+1,j}) - \sin i\,(\sin\beta_{k,j} - \sin\beta_{k+1,j})}{2} \tag{10}$$

The second sum refers to the reflecting valley floor. On the other receiving points similar formulas are valid; for further details refer to Appendix 2.

In the first step simulating single reflection the irradiance appearing in eq. (9) is the sum of the parallel and diffuse sky radiation calculated from eq. (4) and (8) at each grid point. Multiple reflection is obtained by substituting successively between eq. (10) and (9) until convergence to the desired accuracy takes place. Results of each iteration step are summed to give the final irradiance.

3. The Atmospheric Radiation Model

The two-stream method of Zdunkowski et al. [15, 16] is used to obtain flux densities on horizontal receiving elements in atmospheres of nearly arbitrary structure. The method handles absorption by H_2O-vapor, CO_2 and O_3, aerosol and cloud droplets as well as multiple scattering by air and particles. Partial multi-layered cloudiness is treated by a procedure first described in [6] which is based on the idea of maximum overlap between neighboring and statistical independence between separate cloud layers. The spectral integration is carried out by dividing the solar spectrum into four intervals making it possible to handle spectral overlap effects for atmospheric constituents.

Using the development in the previous sections, the flux densities for the inclined and obstructed receiving surfaces may now be obtained from the transformation equations.

The summer and winter midlatitude model atmospheres used in the numerical experiments are taken from [9]. Optical parameters for the rural aerosol model used in this study are due to McClatchey and D'Agati [10] while radiative properties of cloud droplet size distributions are taken from [13]. Between the ground and the cloud aerosol reduces visibility to about 20 km, above the clouds the aerosol effects are assumed to be nearly negligible. The clouds are described in connection with the numerical experiments.

4. Results

The preceeding theory will now be applied to some specific examples: 1. The MESOKLIP-region, 2. the Dischma valley near Davos, Switzerland, 3. along the cross-section of an idealized city street represented by a cavity.

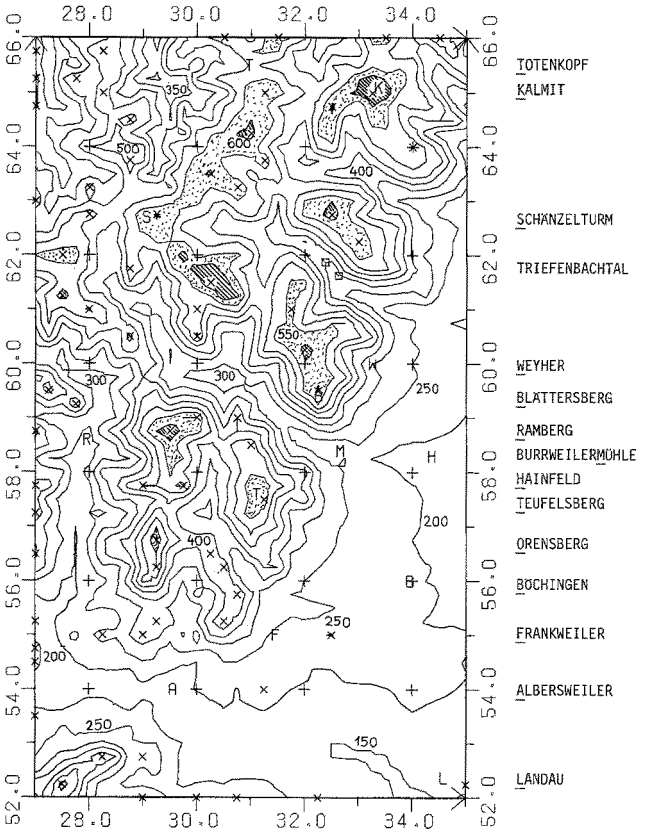

Fig. 3. Computed topography of Haardt-Mountains (mean latitude 49.27°) as western part of the MESOKLIP experiment region. Increments of neighboring iso-height lines are taken as 50 m. The coordinates and the + indicate the 1 km-UTM-grid. (Grid-zone 32U, 100 km-square 4/54.) Crosses mark mountain peaks as well as the dotted regions

4.1 The MESOKLIP-Region

This codename is used to describe an extensive observational program of meteorological parameters obtained in the Oberrheingraben near Neustadt, Germany, in 1979. The applicability of the method is now demonstrated in the Haardt-mountains where slopes up to $i = 40°$ are steep enough to give significant effects. The example is worked out for the time of the summer solstice with a ground albedo of ten percent characteristic of forests.
Due to the low ground albedo and relatively small shadowing angles the contribution of the reflected radiation is rather small so that the single reflection approximation (eq. (5)) is entirely sufficient.

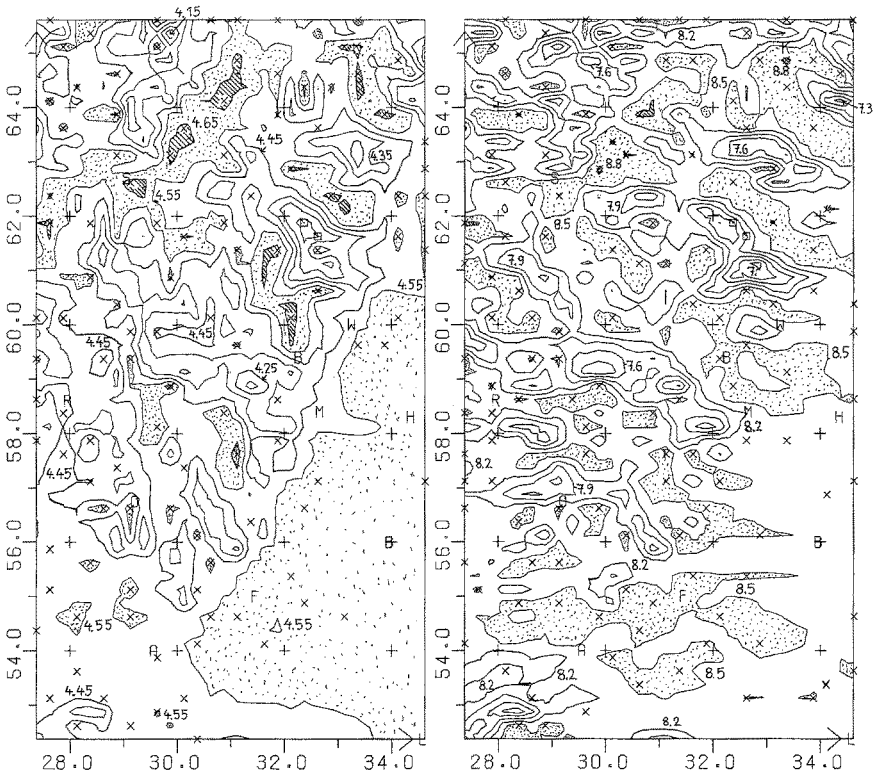

Fig. 4. Contours of daily exposure of solar energy at summer solstice in the region displayed in Fig. 3. High values are dotted and hatched, crosses identify relative maxima. Part left refers to the overcast sky with contour increments of 0.1 kWh/m^2; part right refers to nearly clear sky with increments of 0.3 kWh/m^2

The required topographic data were manually extracted from a map with scale 1:50000 using a grid of 250 m resolution, a reasonable compromise between accuracy and numerical efforts. Height contours calculated in this manner are depicted in Fig. 3 with line spacing of 50 meters.
The method of Escher-Vetter [4] to obtain inclination and azimuthal angles of the receiving elements from squares between grid points in this situation was not sufficiently accurate so that the square was visually divided into two triangles for better results. At the center of gravity of these triangles the shadowing angles α, β for diffuse radiation are approximated by scanning the topography as briefly outlined in the Appendix 1. Diffuse and parallel radiation is then calculated (eqs. 7, 8) for each triangle and results are averaged. Before calculating the parallel radiation a search program similar

to that described by [4] is used to determine if the sun is viewed by the receiving element or not.

For the region displayed in Fig. 3 contours of daily exposure of solar radiation at summer solstice are shown in Fig. 4 for two extreme situations modelling an overcast sky, part left, and a nearly cloud free sky of ten percent cloud cover, part right. The temporal integration is carried out using hourly values. Part left refers to a 400 m thick stratus type cloud with cloud base at 2000 m and an optical depth $\tau = 10$. Part right models thin cloud patches with a total optical depth in the cloudy sections of $\tau = 1.5$ and the same base height. Each case includes the aerosol optical thickness of 0.5.

In part right most solar energy (dotted and hatched regions) is incident on weakly inclined unobstructed slopes facing south or south-east. In contrast, steep slopes facing southerly directions, particularly in valleys, receive less amounts of solar energy since in the morning and late afternoon hours the incoming parallel radiation is strongly reduced. Striking minimum values are observed near the valley bases at slopes facing north. These minima are not only caused by their exposition to the sun but also to a noticeable extent by the obstruction to the sky radiation.

Inspection of Fig. 4 left shows that in case of an overcast sky the shadowing effects of mountains on the diffuse radiation largely determine the amount of solar energy arriving at the ground. This is best demonstrated by the significant depression in the Triefenbach valley identified by the two squares. Moreover, the steep slopes along the line AMW receive less energy than the flat region at the south-easterly corner. Both figures reveal that a failure to sufficiently resolve the valleys in the Haardt mountains may lead to large errors as demonstrated by Table 1. This table compares extreme values of Fig. 4 with the daily sum of solar radiation on a horizontal not obstructed surface at the average height of the mountain region. The table is supplemented by some interesting details of hourly irradiances contained in the computation of Fig. 4. Additionally some data on daily solar exposure are presented for the winter solstice assuming the cloudiness and ground albedo used in Fig. 4 right. Omitting the obstruction effects on sky radiation may cause errors up to 20 percent in the flux densities but only up to ten percent in the daily sums in the MESOKLIP-region.

4.2 The Dischma Valley

This valley has received recent attention in studying the mountain-valley wind systems. Observational data are compiled in [5] but detailed information on the incoming solar radiation along the valley slopes is missing. The mathematical procedure of section 2.3 is suitable to obtain in an approximate manner such important information which is listed for one

Table 1. *Maximum and Minimum Values of Solar Irradiances at Summer Solstice and Daily Exposure in Summer and Winter in the Haardt-Mountains Region, Fig. 3, for Two Extreme Cloudiness Situations.* $D_{\max,\min}$ are the deviations of the extreme values from results obtained for the unobstructed horizontal plane (3rd column) of average altitude

True local time (h)	τ	$F\downarrow+S_h$ (W/m^2)	$(F+S)_{\max}$ (W/m^2)	$(F+S)_{\min}$ (W/m^2)	$D_{\max}$ (%)	$D_{\min}$ (%)
6	1.5	241	430	88	78.5	−63.6
	10	113	114	98	1.2	−12.5
9	1.5	735	936	406	27.5	−44.7
	10	395	402	344	1.6	−12.9
12	1.5	950	1043	689	9.7	−27.5
	10	552	560	482	1.5	−12.6
15	1.5	735	915	407	24.7	−44.5
	10	395	402	345	1.6	−12.8
18	1.5	241	436	91	81.0	−62.4
	10	113	114	98	1.2	−12.5
Exposure		(kWh/m^2)	(kWh/m^2)	(kWh/m^2)	(%)	(%)
21 June	1.5	8.56	8.87	6.93	3.6	−19.0
	10	4.64	4.70	4.06	1.3	−12.6
21 Dec.	1.5	1.08	2.03	0.47	87.4	−56.9

of the observational days (7 August 1980) in Table 2 using some assumed data for input. To give representative results a cross-section in the middle part of the valley is selected, i.e. between the Brunhorn and Börterhorn mountains. The average inclination of the valley walls is taken as 31.6°. The radiation field is calculated using the previously described aerosol now located between the valley floor and the cloud base taken at 3000 m above sea level. The observed average cloudiness of twenty percent is again modelled by thin cloud patches even though any other cloud thickness could be used.

Inspection of the Table 2 shows that the illumination at opposite points is strongly asymmetrical which is mostly due to the orientation of the valley to the sun. The smallest illumination values occur near the valley floor due to shadowing-, obstruction- and extinction effects. The discontinuities at 6 and 18 h local time are due to the shadow boundary occurring at heights of 358 and 269 m above the valley floor, respectively. It is of interest to note that in this case the inclusion of secondary and higher order reflection improves the results by less than one percent due to the small albedo in the lower part of the valley. Furthermore, it should be pointed out that the

Table 2. *Computed Solar Irradiance F+S at 7 August 1980 Along a Cross-Section of the Dischma Valley (1800 m above sea level).* Height of the valley walls is 877 m, width of valley floor is 230 m; $i = 31.6°$, $b_1 = 60°$, $b_2 = -120°$

Height above valley base (m)	Ground albedo (%)	$F+S$ (W/m^2) 6 h	8 h	10 h	12 h	14 h	16 h	18 h
SWW-wall								
789	80	73	241	698	1028	1107	891	410
438	25	78	250	691	1009	1076	848	367
88	15	65	238	662	969	1028	795	55
NEE-wall								
789	85	469	816	894	759	478	157	67
438	35	418	778	872	751	480	168	70
88	15	53	730	836	726	466	165	61
Distance from SWW-wall along valley floor (m)								
25	15	58	536	836	947	834	532	56
115	15	57	535	835	947	834	533	57
205	15	55	532	833	945	833	533	58

assumption of complete isotropy of the reflected radiation (eq. 5, 6) as compared to the model results of Table 2 (different isotropy for each strip, Fig. 2) causes errors up to ±17 percent. The main reasons for this behavior are the strongly varying slope albedo along the valley walls as well as the discontinuity of the parallel solar irradiance caused by obstruction.
To demonstrate the effects of obstruction to the diffuse sky radiation and of multiple reflection on the total irradiance, a winter solstice situation is considered. The ground is snow covered everywhere with ground albedo of 85 percent, cloudiness and aerosol is modelled as in Table 2. Inspection shows that the omission of multiple reflection, otherwise using the complete model, leads to errors exceeding eight percent. For a larger inclination angle the error would be substantially larger as will be discussed in the next section. On the other hand, the neglection of obstruction to sky radiation in the otherwise complete model causes significant errors up to 40 percent.

4.3 The City Street Model

The complete model including multiple reflection makes it possible to calculate irradiances within an arbitrary street cavity. Such data are needed in urban climate modelling. According to Landsberg [8] the relevant

Table 3. *Solar Irradiance F+S at Winter Solstice Along the Cross-Section of the Dischma Valley (data given in Table 2) for 20% Cloud Cover and Uniform Albedo of 85%.* The quantities $\Delta_{\text{mult. ref.}}$, $\Delta_{\text{obstr.}}$ are the relative errors due to neglecting secondary and higher order reflection or obstruction to sky radiation, respectively

Height above valley base (m)	10 h $F+S$ (W/m^2)	$\Delta_{\text{mult. ref.}}$ (%)	$\Delta_{\text{obstr.}}$ (%)	14 h $F+S$ (W/m^2)	$\Delta_{\text{mult. ref.}}$ (%)	$\Delta_{\text{obstr.}}$ (%)
SWW-wall						
789	249	−0.8	0.8	529	−0.5	0.4
438	242	−1.3	4.0	486	−0.9	2.0
88	235	−2.7	11.1	84	−8.3	29.7
0	234	−3.1	13.8	81	−8.3	37.1
NEE-wall						
789	227	−0.8	0.8	99	−0.9	1.9
438	223	−1.3	4.4	113	−1.3	8.7
88	220	−2.7	11.8	108	−2.7	23.1
0	219	−3.2	14.7	95	−3.9	31.7
Distance from the SWW-wall on the floor (m)						
25	233	−1.9	9.8	81	−4.1	26.4
115	233	−1.8	9.7	85	−3.8	24.7
205	233	−1.9	9.8	87	−3.7	24.4

modelling parameter is the narrowness index R, which is the ratio of mean wall height to street width, since extinction effects within not too deep cavities are negligible.

Some results are shown in Fig. 5 for $R = 20/15$ which is quite typical for some Mainz urban sections. Wall and ground albedo are estimated from Dirmhirn [3] as 0.40 and 0.15, respectively. The direction of the street is from SW to NE. The atmospheric situations for simplicity are taken to be identical to the two MESOKLIP-examples at summer solstice. The solid lines refer to the complete model, the broken lines show results including primary reflection only while the dashed-dot-lines pertain to sky radiation F_{sky} in the presence of obstruction. For the clear sky situation (Fig. 5 right) the times are so selected that the shadow boundaries identified by the discontinuities are located on the SE-wall at 9 h and on the ground at 15 h ($\phi_0 = \mp 70°$). In the shadow part on the SE-wall at 9 h and on the ground the omission of higher order reflection causes non-negligible errors. At 15 h the relative errors of neglecting multiple reflection are somewhat

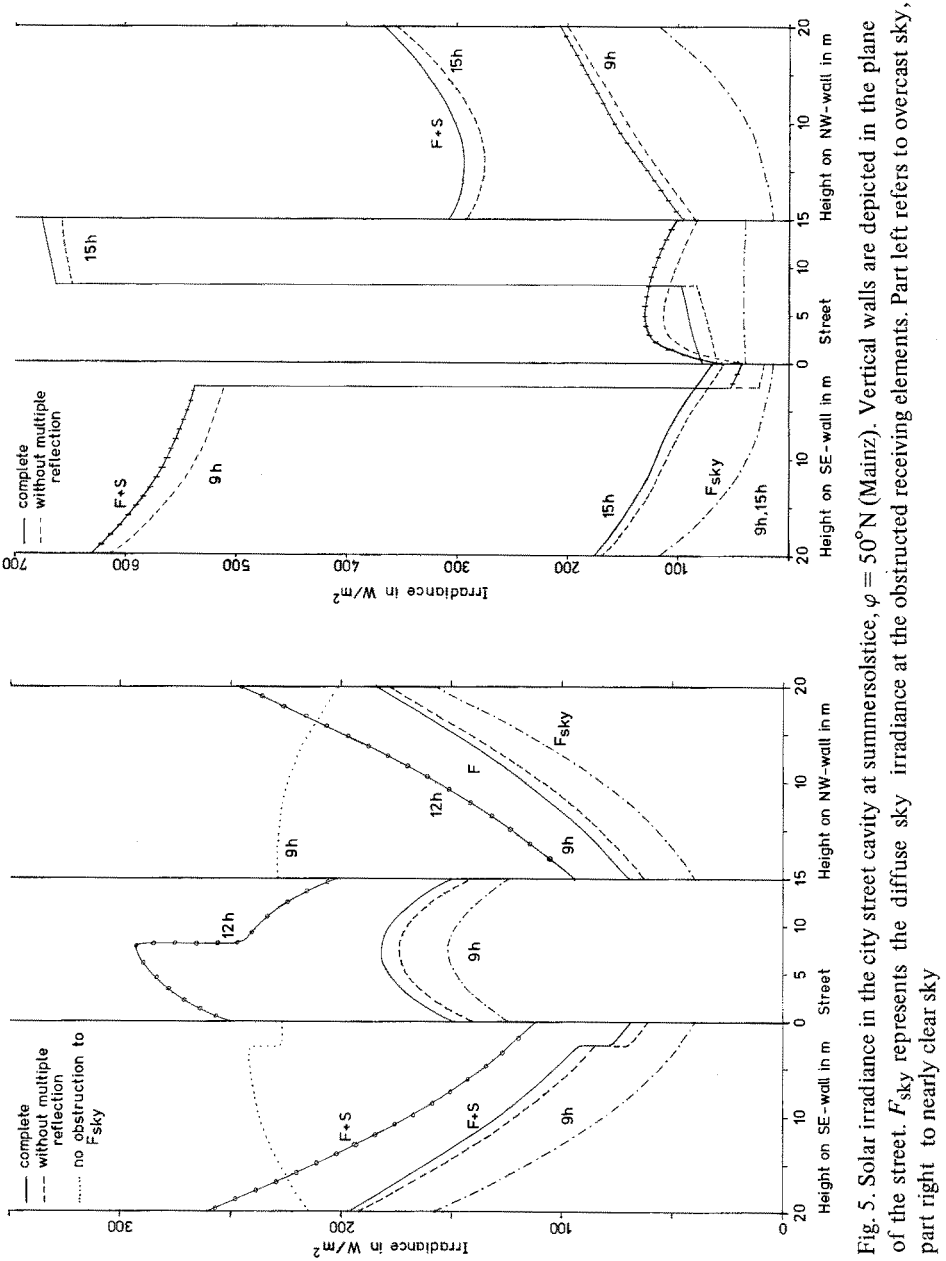

Fig. 5. Solar irradiance in the city street cavity at summersolstice, $\varphi = 50°$N (Mainz). Vertical walls are depicted in the plane of the street. F_{sky} represents the diffuse sky irradiance at the obstructed receiving elements. Part left refers to overcast sky, part right to nearly clear sky

smaller. The sky radiation in the lower part of the cavity at 9 h and 15 h contributes the least energy due to obstruction. If the effect of obstruction on the sky radiation is ignored, the sky irradiance is constant along the walls and on the street giving values of 116 and 167 W/m^2, respectively. Therefore, the omission of obstruction causes errors exceeding one hundred percent.
The example at 9 h in Fig. 5 left demonstrates the domination of obstruction effects on diffuse sky radiation for an overcast sky. Neglecting these effects causes errors up to several hundred percent as indicated by the dotted line. This line is omitted on the ground since its average value here amounts to about 450 W/m^2. Further inspection of the figure shows that the higher order reflection is far less important than in the clear sky situation. Additionally the complete irradiances $F + S$ at noon are also given, identified by circles. The small amount of parallel radiation penetrating the cloud is responsible for the discontinuities.
Finally, it should be noted that in city streets with a larger index of narrowness, e.g. $R = 2$ and the higher albedo of limestone or white painted walls with $A = 0.6$, the higher order reflection becomes very significant. For the overcast sky this physical process contributes up to 30 percent, for the clear sky up to 75 percent to the total result.

5. Summary and Conclusion

A method has been devised for the calculation of parallel and diffuse sky radiation on inclined surfaces in the presence of obstructions. Multiple reflections between obstructions can be accounted for. The calculation scheme has been primarily developed for use in mesoscale-models.
The calculation technique was applied to model the MESOKLIP-region of the Haardt mountains, the Dischma valley and street cavities. In general, it is not possible to omit the effects of obstruction on the diffuse radiation field. Multiple reflection is found to be significant in dealing with street cavities. The geometric consideration may also be used in obtaining longwave flux densities in obstructed regions. For this purpose the radiances in the eqs. (2), (5) and (9) must be replaced and a new set of C_K must be included. The algorithm in section 2.3 needs to be carried out only once describing the thermal radiation received from the emitting black obstacles.
Even though the mathematical formalism looks very complex at first glance, the numerical effort to account for obstruction and multiple reflection is rather limited. The complete geometric calculations using more than fifty grid points in the Dischma valley and in the street cavity require less than five percent of the computer time needed for the evaluation of the radiative transfer code.

Acknowledgement

Gratitude is expressed to the computer center of the University of Mainz for providing computer time.

Appendix 1

The integration limits of partial flux densities F_J in the obstruction model (see eq. 1).

The total solid angle of integration is split in the manner of Z [17] into partial integration domains. In contrast in the present work the solid angles describing downward radiation are subdivided by the shadowing planes defined by α and β into unobstructed and obstructed parts, Fig. 1. The resulting integration limits are summarized in the following table

	ϕ lower	ϕ upper	θ lower	θ upper	ϕ lower	ϕ upper	
F_1	b	$\pi/2+b$	0	$\tan^{-1}(\cot\beta/\cos(\phi-b))$	$3\pi/2+b$	$2\pi+b$	F_2
F_3	b	$\pi/2+b$	$\pi/2$	$\pi-\tan^{-1}(\cot i/\cos(\phi-b))$	$3\pi/2+b$	$2\pi+b$	F_4
F_5	$\pi/2+b$	$\pi+b$	0	$\tan^{-1}(\cot\alpha/-\cos(\phi-b))$	$\pi+b$	$3\pi/2+b$	F_6
F_7	b	$\pi/2+b$	$\tan^{-1}(\cot\beta/\cos(\phi-b))$	$\pi/2$	$3\pi/2+b$	$2\pi+b$	F_8
F_9	$\pi/2+b$	$\pi+b$	$\tan^{-1}(\cot\alpha/-\cos(\phi-b))$	$\tan^{-1}(\cot i/-\cos(\phi-b))$	$\pi+b$	$3\pi/2+b$	F_{10}

In actual situations the shadowing angle β is found by scanning the mountains in five steps of 30° in $(\phi-b)$, beginning with $\phi-b=-60°$. With the five resulting values of the limiting angle θ_s the average angle β is found using

$$\beta=\tan^{-1}\left(\frac{1}{5}\sum_{s=1}^{5}\tan\beta_s\right) \quad \text{with} \quad \tan\beta_s=\cot\theta_s/\cos(\phi-b)_s\ .$$

The same method is applied to the angle α, here $\phi-b$ must be replaced by $\phi-b\pm\pi$. If the resulting $\alpha<i$, α is set equal to i.

Appendix 2

Some geometrical formulas for use in the multiple reflection model.

Refering to eq. 10, for a gridpoint on valley wall 2 the radiances $L_{l,2}$ and L_k must be replaced by $L_{l,1}$ and L_{m-k}, respectively.

The strip-limiting angles are defined by trigonometric relations (obtained from Fig. 2):

$$\beta_{l,j} = \tan^{-1}((Y_l - Y_j)/(W + (Y_l + Y_j)\cot i)) \qquad 1 \leqslant l \leqslant n$$

$\beta_{l,j}$ is the obstruction angle for point Y_j .

$$\beta_{k,j} = \tan^{-1}(-Y_j/(X_k + Y_j \cot i)) \qquad 1 \leqslant k \leqslant m$$

with $\beta_{n,j} \simeq \beta_{m,j}$.

On the receiving point X_k on the valley floor the following formula, analogous to eq. (10), is valid

$$F_{r,k} = \pi \sum_{j=1}^{n-1} L_{j,1} \frac{\cos\alpha_{j+1,k} - \cos\alpha_{j,k}}{2} + \pi \sum_{j=1}^{n-1} L_{j,2} \frac{\cos\beta_{j+1,k} - \cos\beta_{j,k}}{2}$$

with $\alpha_{j,k} = \tan^{-1}(Y_j/(X_k + Y_j \cot i)) \qquad 1 \leqslant j < n,\ 1 \leqslant k \leqslant m$

$\beta_{j,k} = \alpha_{j,m-1+k} \qquad 1 \leqslant j < n,\ 1 \leqslant k \leqslant m$

$\beta_{n,k} = \alpha_{n,k} = 0$

$\alpha_{1,k}$ and $\beta_{1,k}$ represent the obstruction angles of grid points X_k. The shadow boundary to the parallel radiation is given by the relations

$$Y_0 = (H - (W + H\cot i)/G)/(\cot i/G + 1) \qquad \text{if } Y_0 \text{ greater } 0$$

$$X_0 = W + H \cdot \cot i - HG \qquad \text{if } 0 < X_0 < W$$

with $G = |\cos(\phi_0 - b)|/\cot\theta_0$

X_0 is the horizontal distance counted from the valley wall facing the sun, b is the azimuthal angle of wall 1.

References

1. Aida, M.: Urban Albedo as a Function of the Urban Structure – A Model Experiment. Boundary Layer Met. *23*, 405–413 (1982).
2. Aida, M., Gotoh, K.: Urban Albedo as a Function of the Urban Structure – A Two-dimensional Numerical Simulation. Boundary Layer Met. *23*, 415–424 (1982).
3. Dirmhirn, I.: Das Strahlungsfeld im Lebensraum. Frankfurt/Main: Akad. Verlagsges. 1964.
4. Escher-Vetter, H.: Der Strahlungshaushalt des Vernagtferners als Basis der Energiehaushaltsberechnung zur Bestimmung der Schmelzwasserproduktion eines Alpengletschers. Münchener Universitätsschriften, Met. Inst. Nr. 39 (1980).
5. Freitag, C., Hennemuth, B.: DISKUS Gebirgswindexperiment im Dischmatal. Datensammlung Teil 1: Sondierungen. Münchener Universitätsschriften, Met. Inst. Nr. 43 (1981).

6. Geleyn, J. F., Hollingsworth, A.: An Economical Analytical Method for the Computation of the Interaction Between Scattering and Line Absorption of Radiation. Beitr. Phys. Atmosph. *52*, 1–16 (1979).
7. Junghans, H.: Sonnenscheindauer und Strahlungsempfang geneigter Ebenen. Berlin, Abhandlungen d. Meteorol. Dienstes d. DDR *85*, Vol. 11 (1969).
8. Landsberg, H. E.: The Urban Climate. Internat. Geoph. Series, Vol. 28, New York, 1981.
9. McClatchey, R. A., Fenn, R. W., Selby, J. E. A., Volz, F. W., Garing, J. S.: Optical Properties of the Atmosphere. Air Force Cambridge Res. Laboratories, Hanscom Mass., AFCRL-71-0279, Environmental Research Papers No. 354 (1971).
10. McClatchey, R. A., D'Agati, A. P.: Atmospheric Transmission of Laser Radiation: Computer Code LASER. Air Force Cambridge Res. Laboratories, Hanscom Mass., AFGL-TR-78-0029, Environmental Research Papers No. 622 (1978).
11. O'Rourke, P. A., Terjung, W. H.: Urban Parks, Energy Budgets, and Surface Temperatures. Arch. Met. Geoph. Biocl., Ser. B *29*, 327–344 (1981).
12. Terjung, W. H., O'Rourke, P. A.: Energy Input and Resultant Surface Temperatures for Individual Urban Interfaces, Selected Latitudes and Seasons. Arch. Met. Geoph. Biocl., Ser. B *29*, 1–22 (1981).
13. Welch, R. M., Cox, S. K., Davis, J. M.: Solar Radiation and Clouds. Met. Monographs, Amer. Met. Soc. *17* (1980).
14. Welch, R. M., Zdunkowski, W. G.: Improved Approximation for Diffuse Solar Radiation on Oriented Sloping Surfaces. Beitr. Phys. Atmosph. *54*, 362–368 (1981).
15. Zdunkowski, W. G., Panhans, W. G., Welch, R. M., Korb, G.: A Radiation Scheme for Circulation and Climate Models. Beitr. Phys. Atmosph. *55*, 215–238 (1982).
16. Zdunkowski, W. G., Welch, R. M., Korb, G.: An Investigation of the Structure of Typical Two-Stream-Methods for the Calculation of Solar Fluxes and Heating Rates in Clouds. Beitr. Phys. Atmosph. *53*, 147–166 (1980).
17. Zdunkowski, W. G., Welch, R. M., Hanson, R. C.: Direct and Diffuse Solar Radiation on Oriented Sloping Surfaces. Beitr. Phys. Atmosph. *53*, 449–468 (1980).

Authors' address: Prof. Dr. W. Zdunkowski and Chr. Brühl, Johannes Gutenberg Universität, Institut für Meteorologie, Postfach 3980, D-6500 Mainz, Federal Republic of Germany.